Condensate fraction of a resonant Fermi gas with spin-orbit coupling in three and two dimensions

L. Dell'Anna, G. Mazzarella, and L. Salasnich
Dipartimento di Fisica "Galileo Galilei" and CNISM, Università di Padova, I-35122 Padova, Italy
(Received 4 August 2011; published 26 September 2011)

We study the effects of laser-induced Rashba-like spin-orbit coupling along the Bardeen-Cooper-Schrieffer–Bose-Einstein condensate (BCS-BEC) crossover of a Feshbach resonance for a two-spin-component Fermi gas. We calculate the condensate fraction in three and two dimensions and find that this quantity characterizes the crossover better than other quantities, like the chemical potential or the pairing gap. By considering both the singlet and the triplet pairings, we calculate the condensate fraction and show that a large-enough spin-orbit interaction enhances the singlet condensate fraction in the BCS side while suppressing it on the BEC side.

DOI: 10.1103/PhysRevA.84.033633 PACS number(s): 03.75.Ss, 05.30.Fk, 67.85.Lm

I. INTRODUCTION

Over the past several years, the predicted crossover [1–3] from the Bardeen-Cooper-Schrieffer (BCS) state of weakly bound Fermi pairs to the Bose-Einstein condensate (BEC) of molecular dimers has been observed by several experimental groups [4–9]. In two experiments [7,9] the condensate fraction of Cooper pairs [10], which is directly related to the off-diagonal long-range order of the two-body density matrix of fermions [11,12], has been studied with two hyperfine component Fermi vapors of ^{6}Li atoms in the BCS-BEC crossover. The experimental data are in quite good agreement with mean-field theoretical predictions [13,14] and Monte Carlo simulations [15] at zero temperature, while at finite temperature beyond-mean-field corrections are needed [16]. Recently, the condensate fraction in the BCS-BEC crossover for a two-dimensional (2D) Fermi gas [17], and for a three-spin-component Fermi gas with SU(3) symmetry [18], has been theoretically investigated. Remarkably, last year 2D degenerate Fermi gases were experimentally realized for ultracold atoms in a highly anisotropic disk-shaped potential [19].

Quite recently, artificial spin-orbit coupling has been obtained in neutral bosonic systems [20], where the strength of the coupling can be controlled optically, and it has been suggested that the same techniques can be used with ultracold fermions [21,22]. These results have stimulated the theoretical investigation of spin-orbit effects with Rashba [23] and Dresselhaus [24] terms in the BCS-BEC crossover [25–30]. In particular, very recently and independently, several authors have analyzed the evolution from BCS to BEC superfluidity in the presence of spin-orbit coupling for a 3D uniform Fermi gas [25–28] and in the 2D case by use of a perturbative approach [29]. Nevertheless, those papers did not consider the condensate fraction of Fermi pairs.

In the present paper we calculate the chemical potential, the pairing gap, and the condensate fraction along the BCS-BEC crossover both in 3D and 2D as a function of spin-orbit coupling. We show that the two contributions—i.e., those related to the singlet and triplet pairings—to the condensate fraction, separately, characterize the crossover better than the other quantities. Remarkably, a large-enough spin-orbit interaction enhances the singlet contribution to the condensate fraction in the BCS side while suppressing it on the BEC side. The triplet contribution to the condensate grows by increasing the spin-orbit coupling and is larger close to the crossover. On the contrary, the chemical potential and the pair function exhibit no peculiarities along the crossover. Moreover, we find that when the Rashba velocity becomes of the order of the Fermi velocity, there is a value for the dimensionless interaction strength $y = 1/(k_F a_s)$, where k_F denotes the Fermi linear momentum and a_s the interatomic s-wave scattering length, for which the singlet condensate fraction no longer depends on spin-orbit coupling. This nodal point can be promoted as the real point of the crossover. What is observed in three dimensions occurs also in two dimensions where the nodal point occurs when the binding energy ϵ_B is almost equal to the Fermi energy ϵ_F, i.e., $\epsilon_B \approx \epsilon_F$. In 2D the condensate fraction approaches a value of 1 only for extremely large values of the scaled binding energy ϵ_B/ϵ_F.

II. THE MODEL

Let us consider the following Hamiltonian:

$$H = H_0 + H_I, \tag{1}$$

where H_0 is the single-particle Hamiltonian in the presence of Rashba and Dresselhaus terms [23,24], namely

$$H_0 = \sum_{\mathbf{k}} \psi(\mathbf{k})^\dagger \left\{ \frac{\hbar^2 k^2}{2m} + \hbar[v_R(\sigma_x k_y - \sigma_y k_x) + v_D(\sigma_x k_y + \sigma_y k_x)] \right\} \psi(\mathbf{k}), \tag{2}$$

where v_D and v_R are, respectively, the Rashba and Dresselhaus velocities; σ_x and σ_y denote the Pauli matrices in the x and y directions; and $\psi(\mathbf{k})$ is the spinor $\psi(\mathbf{k}) = (\psi_\uparrow(\mathbf{k}), \psi_\downarrow(\mathbf{k}))^T$. H_I is the interaction term given by

$$H_I = -\frac{g}{V} \sum_{\mathbf{k}\mathbf{k}'\mathbf{q}} \psi_\uparrow^\dagger(\mathbf{k}+\mathbf{q}) \psi_\downarrow^\dagger(-\mathbf{k}) \psi_\downarrow(-\mathbf{k}'+\mathbf{q}) \psi_\uparrow(\mathbf{k}'), \tag{3}$$

where $g > 0$, which corresponds to attractive interaction. After defining the order parameter describing the particle pairs, $\Delta = (g/V) \sum_{\mathbf{k}} \langle \psi_\downarrow(-\mathbf{k}) \psi_\uparrow(\mathbf{k}) \rangle$, where V is the volume, at the mean-field level we can decouple the interaction, finding

$$H_I = V \frac{|\Delta|^2}{g} - \sum_{\mathbf{k}} (\Delta^* \psi_\downarrow(-\mathbf{k}) \psi_\uparrow(\mathbf{k}) + \Delta \psi_\uparrow^\dagger(\mathbf{k}) \psi_\downarrow^\dagger(-\mathbf{k})). \tag{4}$$

 ©2011 American Physical Society

Introducing the following multispinor $\Psi(\mathbf{k}) = (\psi_\uparrow(\mathbf{k}), \psi_\downarrow^\dagger(-\mathbf{k}), \psi_\downarrow(\mathbf{k}), \psi_\uparrow^\dagger(-\mathbf{k}))^T$, one can resort to standard path integral formulation at finite temperature obtaining, within a saddle point approximation and after integrating over the fermions [31], the thermodynamic potential

$$\Omega = V\frac{|\Delta|^2}{g} - \frac{1}{2\beta}\sum_{\mathbf{k}\,\omega}\mathrm{Tr}\ln G^{-1} + \sum_{\mathbf{k}}\xi_{\mathbf{k}}, \tag{5}$$

where $\beta = 1/(k_B T)$, where k_B denotes the Boltzmann constant and T the absolute temperature, and G^{-1} is a matrix on the basis of $\Psi(\mathbf{k})$ which reads

$$G^{-1}(\mathbf{k},\omega) = \begin{pmatrix} i\omega + \xi_{\mathbf{k}} & -\Delta & \gamma(\mathbf{k}) & 0 \\ -\Delta^* & i\omega - \xi_{\mathbf{k}} & 0 & -\gamma(-\mathbf{k}) \\ \gamma^*(\mathbf{k}) & 0 & i\omega + \xi_{\mathbf{k}} & \Delta \\ 0 & -\gamma^*(-\mathbf{k}) & \Delta^* & i\omega - \xi_{\mathbf{k}} \end{pmatrix} \tag{6}$$

with $\gamma(\mathbf{k}) = \hbar v_R(k_y + ik_x) + \hbar v_D(k_y - ik_x)$ and $\xi_{\mathbf{k}} = \hbar^2 k^2/2m - \mu$. After summing over the Matsubara frequencies [31] the thermodynamic potential becomes

$$\Omega = V\frac{|\Delta|^2}{g} - \frac{1}{2\beta}\sum_{\mathbf{k}}\sum_{i=1}^{4}\ln(1 + e^{-\beta E_i(\mathbf{k})}) + \sum_{\mathbf{k}}\xi_{\mathbf{k}}, \tag{7}$$

where $E_1(\mathbf{k}) = \sqrt{(\xi_{\mathbf{k}} - |\gamma(\mathbf{k})|)^2 + |\Delta|^2}$, $E_2(\mathbf{k}) = \sqrt{(\xi_{\mathbf{k}} + |\gamma(\mathbf{k})|)^2 + |\Delta|^2}$, $E_3 = -E_1$, and $E_4 = -E_2$. From the thermodynamic formula $N = -\frac{\partial\Omega}{\partial\mu}$ we obtain the equation for the number of particles

$$N = \sum_{\mathbf{k}}\left\{1 - \tanh(\beta E_1(\mathbf{k})/2)\frac{\xi_{\mathbf{k}} - |\gamma(\mathbf{k})|}{2E_1(\mathbf{k})} - \tanh(\beta E_2(\mathbf{k})/2)\frac{\xi_{\mathbf{k}} + |\gamma(\mathbf{k})|}{2E_2(\mathbf{k})}\right\}. \tag{8}$$

The gap equation is, instead, given by

$$\frac{V}{g} = \frac{1}{4}\sum_{\mathbf{k}}\left[\frac{\tanh(\beta E_1(\mathbf{k})/2)}{E_1(\mathbf{k})} + \frac{\tanh(\beta E_2(\mathbf{k})/2)}{E_2(\mathbf{k})}\right], \tag{9}$$

and, finally, the condensate number [12,13] reads

$$N_C = N_0 + N_1, \tag{10}$$

where

$$N_0 = \sum_{\mathbf{k}}|\langle\psi_\uparrow(\mathbf{k})\psi_\downarrow(-\mathbf{k})\rangle|^2 = \frac{|\Delta|^2}{16}\sum_{\mathbf{k}}\left[\frac{\tanh(\beta E_1(\mathbf{k})/2)}{E_1(\mathbf{k})} + \frac{\tanh(\beta E_2(\mathbf{k})/2)}{E_2(\mathbf{k})}\right]^2$$

is the singlet contribution to the condensate, with total spin 0, whereas

$$N_1 = \sum_{\mathbf{k}}|\langle\psi_\uparrow(\mathbf{k})\psi_\uparrow(-\mathbf{k})\rangle|^2 = \frac{|\Delta|^2}{16}\sum_{\mathbf{k}}\left[\frac{\tanh(\beta E_1(\mathbf{k})/2)}{E_1(\mathbf{k})} - \frac{\tanh(\beta E_2(\mathbf{k})/2)}{E_2(\mathbf{k})}\right]^2$$

is the triplet one, with total spin 1.

We are interested in the low temperature regime where the condensate is quite large. Quantitatively we can restrict our study to the zero temperature limit, or, in three dimensions, when at least $2k_B T \ll \Delta$, with Δ now supposed to be a real number. The zero temperature limit is also mandatory for the two dimensional case. In the equations above we have therefore simply $\tanh(\beta E_i(\mathbf{k})/2) \to 1$.

III. THREE DIMENSIONS

Let us consider first the three-dimensional case. Hereafter, we proceed in the same spirit of Ref. [32], generalizing the calculation including the spin-orbit coupling. After rescaling the momenta

$$\mathbf{k} = \frac{\sqrt{2m\Delta}}{\hbar}\mathbf{q} \tag{11}$$

and summing in the continuum ($\sum_{\mathbf{k}} \to \frac{V}{(2\pi)^3}\int d^3\mathbf{k}$) we get, for the number of particles

$$n = \frac{N}{V} = \frac{(2m\Delta)^{3/2}}{(2\pi\hbar)^3} I_N^{3d}(x_0,x_1,x_2), \tag{12}$$

where

$$I_N^{3d}(x_0,x_1,x_2) = \int d^3\mathbf{q}\left[1 - \frac{1}{2}\sum_{r=\pm1}\times\frac{q^2 - x_0 + r\sqrt{x_1^2q_x^2 + x_2^2q_y^2}}{\sqrt{\left(q^2 - x_0 + r\sqrt{x_1^2q_x^2 + x_2^2q_y^2}\right)^2 + 1}}\right], \tag{13}$$

with dimensionless parameters defined as follows:

$$x_0 = \frac{\mu}{\Delta} \tag{14}$$

$$x_1 = 2m\frac{(v_R - v_D)^2}{\Delta} \tag{15}$$

$$x_2 = 2m\frac{(v_R + v_D)^2}{\Delta}. \tag{16}$$

In the continuum limit, due to the choice of a contact potential, the gap equation (9) diverges in the ultraviolet. After regularization [2] the gap equation reads

$$\frac{1}{g} = -\frac{m}{4\pi\hbar^2 a_s} + \frac{1}{V}\sum_{\mathbf{k}}\frac{1}{2(\xi_{\mathbf{k}} + \mu)}, \tag{17}$$

where a_s is the s-wave scattering length between fermions with different spin component. In this way we get

$$y \equiv \frac{1}{k_F a_s} = \frac{1}{3^{1/3}\pi^{5/3}}\frac{I_{a_s}(x_0,x_1,x_2)}{I_N^{3d}(x_0,x_1,x_2)^{1/3}}, \tag{18}$$

where

$$I_{a_s}(x_0,x_1,x_2) = \int d^3\mathbf{q}\left[\frac{1}{q^2} - \frac{1}{2}\sum_{r=\pm1}\times\frac{1}{\sqrt{\left(q^2 - x_0 + r\sqrt{x_1^2q_x^2 + x_2^2q_y^2}\right)^2 + 1}}\right]. \tag{19}$$

Finally, the condensate densities are given by

$$n_s = \frac{N_s}{V} = \frac{(2m\Delta)^{3/2}}{16(2\pi\hbar)^3} I^{3d}_{Ns}(x_0,x_1,x_2), \tag{20}$$

where $s = 0,1$, and

$$I^{3d}_{N_s}(x_0,x_1,x_2) = \int d^3\mathbf{q} \left[\sum_{r=\pm 1} \times \frac{r^s}{\sqrt{\left(q^2 - x_0 + r\sqrt{x_1^2 q_x^2 + x_2^2 q_y^2}\right)^2 + 1}} \right]^2 . \tag{21}$$

We can write also the gap and the chemical potential in terms of the Fermi energy $\epsilon_F = \hbar^2 k_F^2/(2m) = \hbar^2/(2m)(3\pi^2 n)^{2/3}$, therefore

$$\frac{\Delta}{\epsilon_F} = 4\left(\frac{\pi}{3}\right)^{2/3} I^{3d}_N(x_0,x_1,x_2)^{-2/3}, \tag{22}$$

$$\frac{\mu}{\epsilon_F} = 4\left(\frac{\pi}{3}\right)^{2/3} x_0 I^{3d}_N(x_0,x_1,x_2)^{-2/3} . \tag{23}$$

Finally, the spin-orbit velocities can be written in terms of the Fermi velocity

$$\frac{(v_R \mp v_D)^2}{v_F^2} = \left(\frac{\pi}{3}\right)^{2/3} x_{1,2}\, I^{3d}_N(x_0,x_1,x_2)^{-2/3}. \tag{24}$$

We are now in the position to express the two contributions to the condensate fraction

$$\frac{2n_s}{n} = \frac{1}{8}\frac{I^{3d}_{Ns}(x_0,x_1,x_2)}{I^{3d}_N(x_0,x_1,x_2)}, \tag{25}$$

the chemical potential, Eq. (23), and the gap, Eq. (22), in terms of the scattering parameter y, Eq. (18). This is guaranteed, at least heuristically, by the fact that for any point in the space of dimensionless parameters, (x_0,x_1,x_2), there are single values for y, $2n_s/n$, μ/ϵ_F, and Δ/ϵ_F. For $x_1 = x_2 = 0$, namely without spin-orbit couplings, we indeed recover previous analytic results reported in Ref. [32].

The results shown here in the figures are obtained fixing $x_1 = x_2$, namely when only Rashba ($v_D = 0$) or only Dresselhaus ($v_R = 0$) are present. The other special case with $v_R = v_D$ is actually less interesting since in that case the condensate fraction seems to be always suppressed. On the contrary, with only Rashba term (or only Dresselhaus) we observe (see Fig. 1) that, turning on the spin-orbit coupling, the singlet condensate fraction increases in the BCS regime, whereas it decreases in the BEC regime. In particular, for $v_R \gtrsim v_F$ the condensate fraction at $y \approx 0.2$, slightly above the unitarity, which is $2n_0/n \approx 0.7$, does no longer depends on the spin-orbit coupling; see Fig. 2. On the left (BCS side) of this point the singlet condensation is improved by the spin-orbital interaction, whereas on the right (BEC side) this condensation is suppressed. The triplet condensate fraction, instead, decreases in both the BCS and BEC limits, whereas it is sizable close to the crossover, exhibiting a nonmonotonic

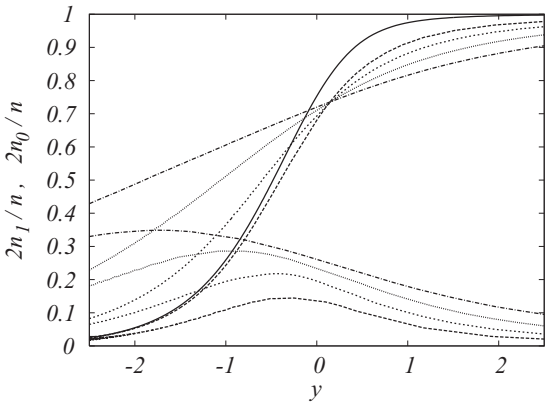

FIG. 1. Singlet (n_0, upper curves) and triplet (n_1, lower curves) condensate fractions of the 3D Fermi gas as functions of the dimensionless interaction strength $y = 1/(k_F a_s)$ for different values of Rashba velocity, $(v_R/v_F)^2 = 0$ (solid line), 0.5 (long-dashed line), 1 (short-dashed line), 2 (dotted line), and 4 (dashed-dotted line).

behavior. On the contrary, the chemical potential μ (upper panel of Fig. 3) is shifted toward negative values in both the regimes, while the pair function Δ (lower panel of Fig. 3) is enhanced both in the BCS side and in the BEC one, although, in the latter, the enhancement is less pronounced. These last quantities, therefore, unlike the condensate fraction, exhibit no peculiarities across the crossover.

IV. TWO DIMENSIONS

In two dimensions the regularization of the gap equation differs, with a bound state always present [33]. With ϵ_B as the binding energy, we have, therefore,

$$\frac{1}{g} = \frac{1}{V}\sum_{\mathbf{k}} \frac{1}{2(\xi_{\mathbf{k}} + \mu) + \epsilon_B}, \tag{26}$$

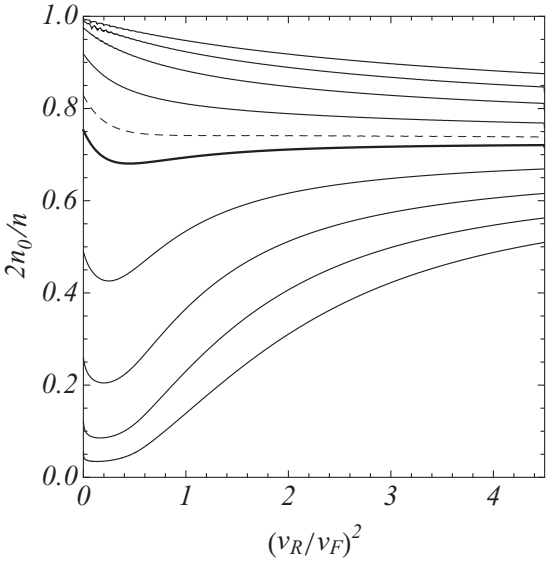

FIG. 2. Singlet condensate fraction of the 3D Fermi gas as a function of $(v_R/v_F)^2$ for $y = -2,-1.5,-1,-0.5,0,0.18,0.5,1,1.5,2$ (corresponding to the curves from below). The solid thicker line is for $y = 0$. The dashed line is when $y \approx 0.2$, below this value all the curves have a minimum, while above it they always decrease.

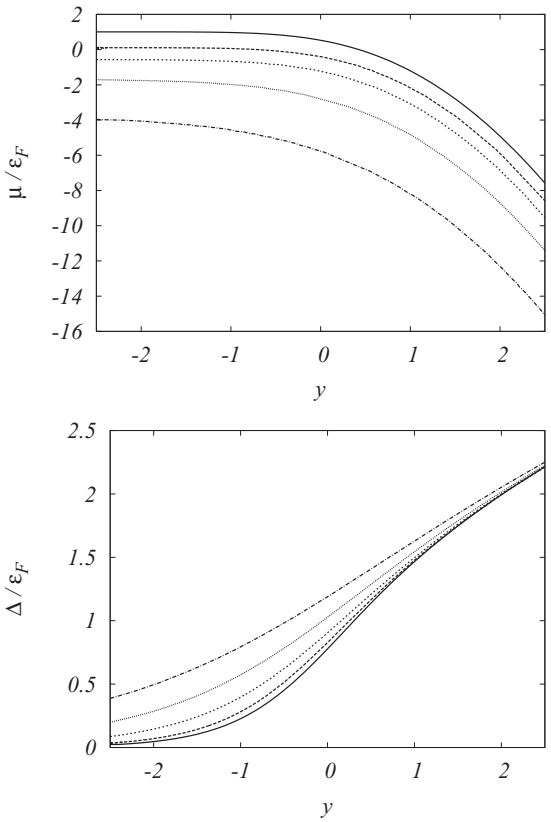

FIG. 3. 3D Fermi gas: Chemical potential μ (upper panel) and pair function Δ (lower panel), both in units of ϵ_F, as a function of the dimensionless interaction strength $y = 1/(k_F a_s)$ for different values of $(v_R/v_F)^2$ (the same ones as in Fig. 1, with same line types).

which, after rescaling the momenta as in Eq. (11) and integrating, leads to

$$\frac{1}{g} = \frac{m}{4\pi\hbar^2} \ln\left(\frac{2\Lambda^2}{\epsilon_B/\Delta} + 1\right), \tag{27}$$

where Λ is the ultraviolet momentum cutoff. On the other hand, Eq. (9) holds, where now the sum is over momenta in two dimensions, and, therefore, we have

$$\frac{1}{g} = \frac{m}{(2\pi\hbar)^2} I_g(x_0,x_1,x_2) \tag{28}$$

with

$$I_g(x_0,x_1,x_2) = \frac{1}{2}\int^{\Lambda} d^2\mathbf{q} \left[\sum_{r=\pm 1} \times \frac{1}{\sqrt{\left(q^2 - x_0 + r\sqrt{x_1^2 q_x^2 + x_2^2 q_y^2}\right)^2 + 1}}\right]. \tag{29}$$

From this expression we derive the binding energy

$$\frac{\epsilon_B}{\Delta} = \lim_{\Lambda\to\infty} \frac{2\Lambda^2}{\exp[I_g(x_0,x_1,x_2)/\pi] - 1}, \tag{30}$$

which actually does not depend on the cutoff since I_g has a logarithmic divergence in the ultraviolet which cancels exactly

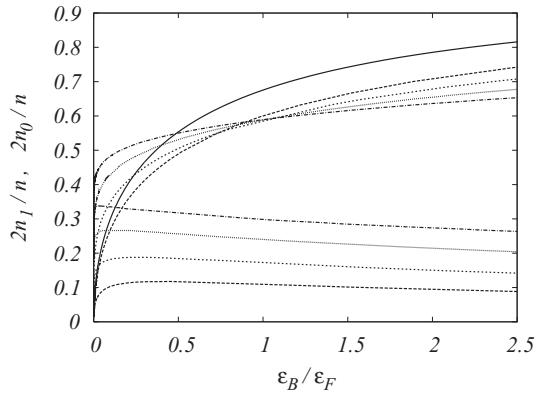

FIG. 4. Singlet (n_0, upper curves) and triplet (n_1, lower curves) condensate fractions of the 2D Fermi gas as functions of the binding energy ϵ_B, in units of the Fermi energy ϵ_F, for different values of Rashba velocity, $(v_R/v_F)^2 = 0$ (solid line), 0.5 (long-dashed line), 1 (short-dashed line), 2 (dotted line), and 4 (dashed-dotted line).

the factor Λ^2. In the absence of spin-orbit, $x_1 = x_2 = 0$, we recover, in fact, the known result $\epsilon_B/\Delta = \sqrt{x_0^2+1} - x_0$ [32].

As in the the three-dimensional case, the quantities we consider are the following:

$$\frac{2n_s}{n} = \frac{1}{8}\frac{I_{Ns}^{2d}(x_0,x_1,x_2)}{I_N^{2d}(x_0,x_1,x_2)}, \tag{31}$$

$$\frac{\mu}{\epsilon_F} = \frac{2\pi x_0}{I_N^{2d}(x_0,x_1,x_2)}, \tag{32}$$

$$\frac{\Delta}{\epsilon_F} = \frac{2\pi}{I_N^{2d}(x_0,x_1,x_2)}, \tag{33}$$

as functions of ϵ_B/ϵ_F where now $\epsilon_F = \hbar^2\pi n/m$ is the Fermi energy in two dimensions. The integrals I_N^{2d} and I_{Ns}^{2d} are

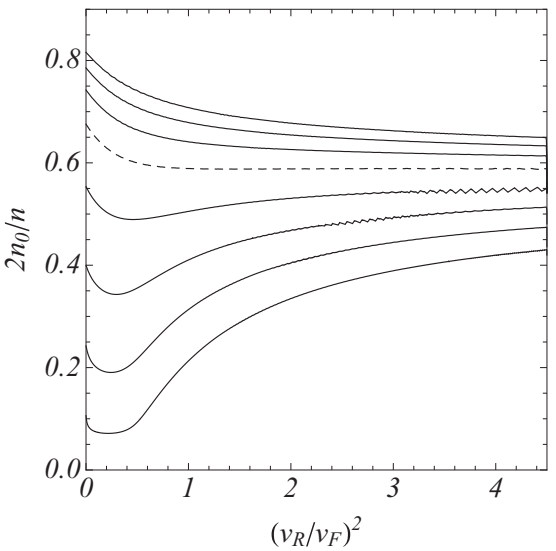

FIG. 5. Singlet condensate fraction of the 2D Fermi gas as a function of $(v_R/v_F)^2$ for $\epsilon_B/\epsilon_F = 0.01, 0.06, 0.2, 0.5, 1, 1.5, 2, 2.5$ (corresponding to the curves from below). The dashed line is when $\epsilon_B/\epsilon_F \approx 1$; below this value all the curves have a minimum, whereas, above it, they always decrease.

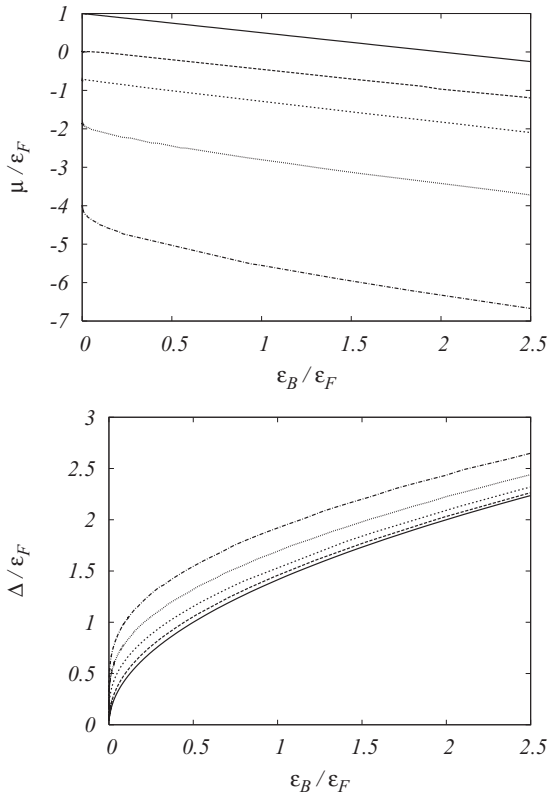

FIG. 6. 2D Fermi gas: Chemical potential μ (upper panel) and pair function Δ (lower panel), both in units of ϵ_F, as a function of the binding energy ϵ_B (in units of ϵ_F) for different values of $(v_R/v_F)^2$ (the same ones as in Fig. 4 with same line types).

the same ones as in Eqs. (13) and (21) but defined in two dimensions ($d^3\mathbf{q} \to d^2\mathbf{q}$).

Experimentally, the realization of a 2D system can be obtained by a strong harmonic confinement in one direction, i.e., $\omega_z \gg \omega_x, \omega_y$; therefore, one can link the tunable 3D scattering length a_s to the two-body binding energy in 2D. Introducing, conveniently, the confining length $\ell_z = \sqrt{h/m\omega_z}$, one finds, in fact, $\ln(\epsilon_B/\hbar\omega_z) \sim \ell_z/a_s$ (for more details see Refs. [34,35]).

Again, we focus our attention to the case with only Rashba (or, equivalently, only Dresselhaus) term, i.e., $x_1 = x_2$. Also in this case, as in the three-dimensional one, the spin-orbit produces interesting effects in the condensate fraction, showing a nodal point at $\epsilon_B \approx \epsilon_F$, set in when $v_R \simeq v_F$, see Figs. 4 and 5, in the neighborhood of which the slope of the curve decreases. As a result, the spin-orbit coupling promotes the singlet condensation in the BCS side and suppresses it on the BEC side. We observe that, contrary to the 3D case, in 2D the condensate fraction approaches the value of 1 only for an extremely large interaction strength, i.e., for $\epsilon_B/\epsilon_F \gg 1$. Again, the chemical potential μ is pushed toward more negative values (see the upper panel of Fig. 6). For small spin-orbit coupling, and $\epsilon_B \to 0$, one recovers the known perturbative result, $\mu \simeq \epsilon_F - mv_R^2/2$. The pairing gap Δ (lower panel of Fig. 6) is, instead, increased by the Rashba spin-orbit interaction in the whole crossover.

V. CONCLUSIONS

We have studied the evolution of BCS superconductors to BEC superfluids in the presence of an artificial spin-orbit coupling of Rashba and/or Dresselhaus type in two and three dimensions. We have shown that, unlike the chemical potential and the pairing gap which exhibit no particular behaviors at the crossover, the condensate fraction is very peculiar. The condensation of singlet pairs, in fact, is promoted by Rashba coupling in the BCS regime, whereas it is suppressed in the BEC regime. In the middle, both in three and in two dimensions and for large-enough Rashba spin-orbit coupling, there is a nodal point where the curves of the condensate fraction cross each other, and, for this reason, this can be considered the putative point of the crossover. On the other hand, the triplet contribution to the condensate fraction has not a monotonic behavior as a function of the scattering parameter, swelling up close to the crossover. Because in our calculations we have used the mean-field theory, it is important to stress that Monte Carlo simulations have shown that, at zero temperature, beyond-mean-field effects are negligible in the BCS side of the BCS-BEC crossover, whereas they become relevant in the deep BEC side [15,35]. In conclusion, we think that our results can be of interest for future experiments with artificial gauge potentials in degenerate gases made of alkali-metal atoms.

ACKNOWLEDGMENTS

The authors thank B. Huang and K. Zhou for useful comments. L.D. thanks the International School for Advanced Studies, SISSA, Trieste, for hospitality and facilities during the completion of this work.

[1] D. M. Eagles, Phys. Rev. **186**, 456 (1969).
[2] A. J. Leggett, in *Modern Trends in the Theory of Condensed Matter*, edited by A. Pekalski and J. Przystawa (Springer, Berlin, 1980), p. 13.
[3] P. Noziers and S. Schmitt-Rink, J. Low Temp. Phys. **59**, 195 (1985).
[4] M. Greiner, C. A. Regal, and D. S. Jin, Nature (London) **426**, 537 (2003).
[5] C. A. Regal, M. Greiner, and D. S. Jin, Phys. Rev. Lett. **92**, 040403 (2004).
[6] J. Kinast, S. L. Hemmer, M. E. Gehm, A. Turlapov, and J. E. Thomas, Phys. Rev. Lett. **92**, 150402 (2004).
[7] M. W. Zwierlein, C. A. Stan, C. H. Schunck, S. M. F. Raupach, A. J. Kerman, and W. Ketterle, Phys. Rev. Lett. **92**, 120403 (2004); M. W. Zwierlein, C. H. Schunck, C. A. Stan, S. M. F. Raupach, and W. Ketterle, *ibid.* **94**, 180401 (2005).
[8] C. Chin *et al.*, Science **305**, 1128 (2004); M. Bartenstein, A. Altmeyer, S. Riedl, S. Jochim, C. Chin, J. H. Denschlag, and R. Grimm, Phys. Rev. Lett. **92**, 203201 (2004).

[9] Y. Inada, M. Horikoshi, S. Nakajima, M. Kuwata-Gonokami, M. Ueda, and T. Makaiyama, Phys. Rev. Lett. **101**, 180406 (2008).
[10] C. N. Yang, Rev. Mod. Phys. **34**, 694 (1962).
[11] O. Penrose, Philos. Mag. **42**, 1373 (1951); O. Penrose and L. Onsager, Phys. Rev. **104**, 576 (1956).
[12] C. E. Campbell, in *Condensed Matter Theories* (Nova Science, New York, 1997), Vol. 12, p. 131.
[13] L. Salasnich, N. Manini, and A. Parola, Phys. Rev. A **72**, 023621 (2005).
[14] G. Ortiz and J. Dukelsky, Phys. Rev. A **72**, 043611 (2005).
[15] G. E. Astrakharchik, J. Boronat, J. Casulleras, and S. Giorgini, Phys. Rev. Lett. **93**, 200404 (2004).
[16] Y. Ohashi and A. Griffin, Phys. Rev. A **72**, 063606 (2005); N. Fukushima, Y. Ohashi, E. Taylor, and A. Griffin, *ibid.* **75**, 033609 (2007).
[17] L. Salasnich, Phys. Rev. A **76**, 015601 (2007).
[18] L. Salasnich, Phys. Rev. A **83**, 033630 (2011).
[19] K. Martiyanov, V. Makhalov, and A. Turlapov, Phys. Rev. Lett. **105**, 030404 (2010).
[20] Y. J. Lin, K. Jimenez-Garcia, and I. B. Spielman, Nature **471**, 83 (2011).
[21] J. Dalibard, F. Gerbier, G. Juzeliunas, and P. Ohberg, e-print arXiv:1008.5378v1.
[22] M. Chapman and C. A. R. Sa de Melo, Nature **471**, 41 (2011).
[23] Y. A. Bychkov and E. I. Rashba, J. Phys. C **17**, 6029 (1984).
[24] G. Dresselhaus, Phys. Rev. **100**, 580 (1955).
[25] M. Gong, S. Tewari, and C. Zhang, e-print arXiv:1105.1796.
[26] Z-Q. Yu and H. Zhai, e-print arXiv:1105.2250.
[27] H. Hu, L. Jiang, X-J. Liu, and H. Pu, e-print arXiv:1105.2488 (2011).
[28] Li Han and C. A. R. Sa de Melo, e-print arXiv:1106.3613.
[29] G. Chen, M. Gong, and C. Zhang, e-print arXiv:1107.2627.
[30] M. Burrello and A. Trombettoni, e-print arXiv:1108.0839.
[31] H. T. C. Stoof, B. M. Dennis, and K. Gubbels, *Ultracold Quantum Fields* (Springer, Berlin, 2009).
[32] M. Marini, F. Pistolesi, and G. C. Strinati, Eur. Phys. J. **1**, 151 (1998).
[33] M. Randeria, J.-M. Duan, and L.-Y. Shieh, Phys. Rev. B **41**, 327 (1990).
[34] L.-K. Lim, C. M. Smith, and H. T. C. Stoof, Phys. Rev. A **78**, 013634 (2008).
[35] G. Bertaina and S. Giorgini, Phys. Rev. Lett. **106**, 110403 (2011).